Available online at www.sciencedirect.com
ScienceDirect
Journal of Sound and Vibration 308 (2007) 794–804
JOURNAL OF SOUND AND VIBRATION
www.elsevier.com/locate/jsvi

Impact analysis of a rotating beam due to particle mass collision

Hong Seok Lim, Sung Hun Kwon, Hong Hee Yoo*

School of Mechanical Engineering, Hanyang University, 17 Haengdang-Dong Sungdong-Gu, Seoul 133-791, Republic of Korea

Accepted 28 March 2007
The peer review of this article was organised by the Guest Editor
Available online 21 May 2007

Abstract

Rotating beam structures can be found in engineering examples like turbine and helicopter blades. During their operation, collision between a blade and a particle mass may occur unexpectedly. The impact caused by such collision often results in significant structural damage. Therefore, the collision effect on the dynamic response of the structure should be estimated accurately for a reliable design of the structure. In the present study, a linear hybrid deformation modeling method along with the Kane's method is employed to derive the equations of motion. The impulse created by the collision between the rotating beam and the particle can be obtained by using the impulse and momentum principle, where a coefficient of restitution is employed. Substituting the impulse into the equations of motion, the dynamic response of the beam can be obtained. Effects of the particle mass size, the collision location, the coefficient of restitution, and the angular motion of the beam on the dynamic response characteristics of rotating beams are investigated through numerical study.

1. Introduction

Rotating cantilever beam-like structures can be found in practical engineering examples such as turbo machine blades, aircraft blades and golf clubs. Rotating motion of a beam induces the variation of the system bending stiffness that causes the variation of dynamic characteristics. However, particle collisions against rotating structures may often occur during their operation (collisions between a bird and a rotating blade or between a ball and a golf club head). These collisions usually result in excessive deflection and stress in the collided structures, that affect the product life of the structures. Therefore, the dynamic characteristics of a rotating structure which is collided by a particle mass should be carefully identified for a reliable design of the structure.

Studies on the dynamic characteristics of flexible structures undergoing rotating motions were done by many previous researchers. Southwell [1] and Schilhansl [2] provided early theoretical background on the subject and many numerical works (see, for instance, Putter and Manor [3], Bhat [4] and Yoo, Ryan and Scott [5]) have followed. In these papers, beam structures undergoing rotating motions were only studied without considering the impact effect. In most of the papers in which the impact effect was considered, stationary structures were only studied (see, for instance, Solberg and Papadopoulos [6] and Demkowicz and Bajer [7]).

*Corresponding author. Tel.: +82 2 2220 0446; fax: +82 2 2293 5070.
E-mail addresses: beyondlimits@hanmail.net (H.S. Lim), axlkwon@korea.com (S.H. Kwon), hhyoo@hanyang.ac.kr (H.H. Yoo).

0022-460X/$ - see front matter © 2007 Elsevier Ltd. All rights reserved.
doi:10.1016/j.jsv.2007.03.052

The purpose of the present study is to propose a modeling method by which the transient responses and the modal characteristics of rotating cantilever beam undertaking impact can be obtained. Using the modeling method, the effects of the particle mass size, the location of collision, the coefficient of restitution and the rotating speed on the transient responses and the modal characteristics of rotating cantilever beams will be investigated and discussed through numerical studies.

This paper consists of four sections. Following this section, the equations of motion of a rotating cantilever beam, which is collided with a particle are derived. Hybrid deformation variables and Kane's method are employed to derive the equations of motion. In the third section, numerical results obtained by employing the equations of motion are exhibited and discussions related to the results are given. Especially, the effects of particle mass size, angular speed of beam, impact location on the dynamic characteristics of the rotating beam are investigated. Finally, conclusions are made in the final section.

2. Formulation for the modal analysis

Fig. 1 shows a cantilever beam which is characterized by natural length L. The beam is attached to a rigid hub $\hat{A}$ that undergoes rotational motion with a constant angular velocity ω_3. Collision between a rotating beam and a particle mass may occur in the bending direction of the beam at an arbitrary time t_I. The elastic displacement of a generic point P of the beam can be expressed by using Cartesian deformation variables u_1 and u_2 that are orthogonal to each other. The mass per unit length, the Poisson's ratio, the Young's modulus, the radius of hub, the area moment of the beam cross-section and the particle mass size are denoted by symbols ρ_b, v, E, r, I and m, respectively.

In the present work, equations of motion are derived by employing hybrid deformation variables instead of Cartesian deformation variables. By employing the hybrid deformation variables one can capture the motion induced stiffening effect with a linear modeling which cannot be captured only with the set of classical Cartesian deformation variables. The hybrid deformation variable modeling method is well described in Ref. [5].

In hybrid deformation variable modeling method, two deformation variables s and u_2 can be approximated employing the Rayleigh–Ritz method as follows:

$$s = \sum_{i=1}^{\mu_1} \phi_{1i}(x) q_{1i}(t), \tag{1}$$

$$u_2 = \sum_{i=1}^{\mu_2} \phi_{2i}(x) q_{2i}(t), \tag{2}$$

where μ_1 and μ_2 are the numbers of generalized coordinates for the deformation variables s and u_2, respectively.

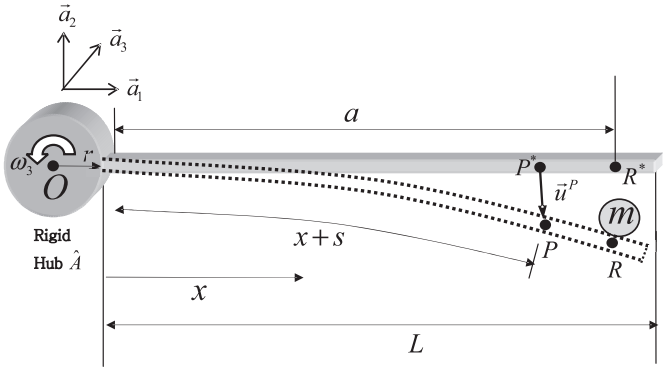

Fig. 1. Configuration of a rotating cantilever beam and a particle.

The equations of motion can be derived by using Kane's method. With the velocity $\vec{v}^P$ and the acceleration $\vec{a}^P$ of a generic point P, the generalized inertia forces F_i^* can be expressed as follows:

$$F_i^* = -\int_0^L \rho_b \left(\frac{\partial \vec{v}^P}{\partial \dot{q}_{1i}}\right) \cdot \vec{a}^P \, \mathrm{d}x \quad (i = 1, 2, \ldots, \mu_1),$$
$$F_{i+\mu_1}^* = -\int_0^L \rho_b \left(\frac{\partial \vec{v}^P}{\partial \dot{q}_{2i}}\right) \cdot \vec{a}^P \, \mathrm{d}x \quad (i = 1, 2, \ldots, \mu_2). \tag{3}$$

The generalized active forces F_i consist of F_i^U (which results from the strain energy of beam U) and F_i^I (which results from the external impulsive force induced by the collision). In the equations of motion to be derived, the impulsive force can be expressed with the impulse magnitude and a Dirac delta function $\delta(t - t_I)\delta(x - a)$. Thus, the components of the generalized active forces can be expressed as follows:

$$F_i^U = -\frac{\partial U}{\partial q_{1i}} = -\left(\int_0^L \mathrm{EA}\phi_{1i,x}\phi_{1j,x} \, \mathrm{d}x\right) q_{1j} \quad (i = 1, 2, \cdots, \mu_1)$$
$$F_{i+\mu_1}^U = -\frac{\partial U}{\partial q_{2i}} = -\left(\int_0^L \mathrm{EI}\phi_{2i,xx}\phi_{2j,xx} \, \mathrm{d}x\right) q_{2j} \quad (i = 1, 2, \cdots, \mu_2) \tag{4}$$

$$F_i^I = 0 \quad (i = 1, 2, \ldots, \mu_1)$$
$$F_{i+\mu_1}^I = \int_0^L \left(\frac{\partial \hat{v}^P}{\partial \dot{q}_{2i}}\right)(-I_{mp}\delta(t - t_I)\delta(x - a))\hat{a}_2 \, \mathrm{d}x$$
$$= -I_{mp}\delta(t - t_I)\phi_{2i}(a) \quad (i = 1, 2, \ldots, \mu_2), \tag{5}$$

$$F_i = F_i^U + F_i^I \quad (i = 1, 2, \ldots, \mu_1 + \mu_2), \tag{6}$$

where a subscript following a comma indicates the partial differentiation with respect to the subscript. For instance, $\phi_{i,xx}$ denotes the double differentiation of ϕ_i with respect to x.

Finally, the equations of motion can be derived by summing up the generalized inertia forces and the generalized active forces

$$F_i + F_i^* = 0 \quad (i = 1, 2, \ldots, \mu_1 + \mu_2). \tag{7}$$

Thus, the equations of motion in stretching and bending direction are derived as follows:

$$\sum_{j=1}^{\mu_1}\left[\left(\int_0^L \rho_b\phi_{1i}\phi_{1j} \, \mathrm{d}x\right)\ddot{q}_{1j} + \left\{\left(\int_0^L \mathrm{EA}\phi_{1i,x}\phi_{1j,x} \, \mathrm{d}x\right) - \omega_3^2\left(\int_0^L \rho_b\phi_{1i}\phi_{1j} \, \mathrm{d}x\right)\right\}q_{1j}\right]$$
$$= r\omega_3^2\left(\int_0^L \rho_b\phi_{1i} \, \mathrm{d}x\right) - \omega_3^2\left(\int_0^L \rho_b x\phi_{1i} \, \mathrm{d}x\right) \quad (i = 1, 2, \ldots, \mu_1) \tag{8}$$

$$\sum_{j=1}^{\mu_2}\left[\left(\int_0^L \rho_b\phi_{2i}\phi_{2j} \, \mathrm{d}x\right)\ddot{q}_{2j} + \left\{\left(\int_0^L \mathrm{EI}\phi_{2i,xx}\phi_{2j,xx} \, \mathrm{d}x\right) - \omega_3^2\left(\int_0^L \rho_b\phi_{2i}\phi_{2j} \, \mathrm{d}x\right)\right.\right.$$
$$\left.\left. + r\omega_3^2\left(\int_0^L \rho_b(L - x)\phi_{2i,x}\phi_{2j,x} \, \mathrm{d}x\right) + \omega_3^2\left(\frac{1}{2}\int_0^L \rho_b(L^2 - x^2)\phi_{2i,x}\phi_{2j,x} \, \mathrm{d}x\right)\right\}q_{2j}\right]$$
$$= -I_{mp}\delta(t - t_I)\phi_{2i}(a) - r\dot{\omega}_3\left(\int_0^L \rho_b\phi_{2i} \, \mathrm{d}x\right) - \dot{\omega}_3\left(\int_0^L \rho_b x\phi_{2i} \, \mathrm{d}x\right) \quad (i = 1, 2, \ldots, \mu_2), \tag{9}$$

where ω_3 denotes the angular speed of the rigid hub.

To obtain the impulse, the following equation involved with the coefficient of restitution is employed:

$$e = \frac{\bar{v}_m - \bar{v}_b(a)}{v_b(a) - v_m}, \tag{10}$$

where subscripts b and m denote the beam and the particle, respectively. For instance, v_b and v_m denote the velocities of the beam and the particle before collision and $\bar{v}_b$ and $\bar{v}_m$ denote the velocities of the beam and the particle after collision. In this study, a simple method to estimate the structural response due to impact is employed with a constant coefficient of restitution. Recently, more complicated models to estimate the response of elastic bodies due to impact were introduced (see Refs. [8–10]). However, a simple model for the impact is employed in this study since the main purpose of the present study is to estimate the structural response of a rotating beam with an impact. So, the accuracy of the impact model itself is not the major concern of the study.

As the collision is given in the bending direction, the equations of motion of the bending direction are to be solved. The velocity of the particle before collision is zero. Since the collision only causes the instant change of velocity, the initial conditions can be expressed as follows:

$$q_{2i}(t_I) = q_{2i}(t_I+). \tag{11}$$

Now the velocity of beam in the bending direction before and after collision can be expressed as follows:

$$v_b(x) = \sum_{i=1}^{\mu_2} \phi_{2i}(x)\dot{q}_{2i}(t_I) + \omega_3(r+x), \tag{12}$$

$$\bar{v}_b(x) = \sum_{i=1}^{\mu_2} \phi_{2i}(x)\dot{q}_{2i}(t_I+) + \omega_3(r+x). \tag{13}$$

To obtain $\dot{q}_{2i}(t_I+)$, the both sides of Eq. (9) are integrated from $t = t_I$ to $t = t_I+$. Then, $\dot{q}_{2i}(t_I+)$ can be obtained as follows:

$$\sum_{j=1}^{\mu_2}\left(\int_0^L \rho_b\phi_{2i}\phi_{2j}\,\mathrm{d}x\right)[\dot{q}_{2j}(t_I+) - \dot{q}_{2j}(t_I)] = -I_{mp}\phi_{2i}(a) \quad (i = 1, 2, \ldots, \mu_2). \tag{14}$$

The impulse between the rotating beam and the particle can be obtained by using the impulse and momentum principle as follows:

$$I_{mp} = m(\bar{v}_m - v_m). \tag{15}$$

Now solving Eqs. (10), (14), and (15) simultaneously, the velocity of the particle mass after the collision can be obtained as follows:

$$\bar{v}_m = \frac{(e+1)\left[\omega_3(r+a) + \sum_{i=1}^{\mu_2}\phi_{2i}(a)\dot{q}_{2i}(t_I)\right]}{1 + (m/\rho_b L)\sum_{i=1}^{\mu_2}\phi_{2i}(a)\phi_{2i}(a)}. \tag{16}$$

Now substituting the impulse given in Eq. (15) into Eq. (14), one can obtain $\dot{q}_{2i}(t_I+)$. Using this initial condition along with Eq. (11), the equations of motion can be solved to obtain the response of the beam after the collision.

3. Numerical results

In this section, numerical results are obtained by using the equations of motion, which are derived in the previous section. The employed mode functions are the eigenfunctions of the bending vibrations of the stationary cantilever beam. Table 1 shows the properties of the beam.

Table 1
Properties of the beam

L (m)	I (m^4)	ρ_b (kg/m)	E (N/m^2)	r (m)
5.0	1.333×10^{-8}	1.2	7×10^{10}	0.0

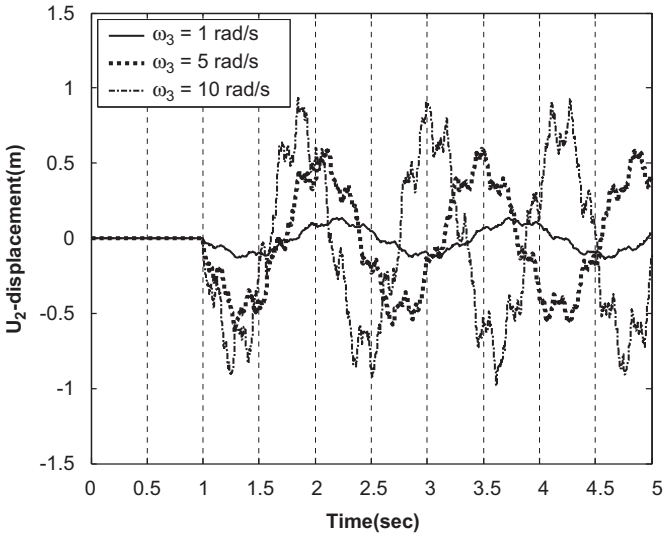

Fig. 2. Variation of beam tip deflection induced by the impact with different angular velocity ($e = 1$, $a = 5\,\text{m}$, $t_I = 1\,\text{s}$, $m = 0.1\,\text{kg}$): —— $\omega_3 = 1\,\text{rad/s}$, ····· $\omega_3 = 5\,\text{rad/s}$, –·– $\omega_3 = 10\,\text{rad/s}$.

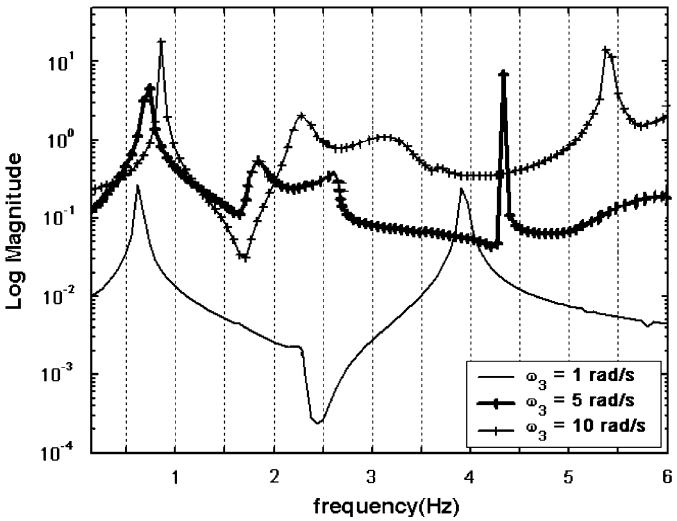

Fig. 3. Energy distribution versus frequency after the impact with different angular velocity ($e = 1$, $a = 5\,\text{m}$, $t_I = 1\,\text{s}$, $m = 0.1\,\text{kg}$): —— $\omega_3 = 1\,\text{rad/s}$, ——┼—— $\omega_3 = 5\,\text{rad/s}$, ——┼—— $\omega_3 = 10\,\text{rad/s}$.

Fig. 2 shows the lateral deflection of the rotating beam undergoes constant angular velocity at the tip with different values of angular velocity. Seven bending modes are employed to obtain the results. As shown in the figure, the peak amplitude increases as the angular velocity increases. Such phenomenon results from the fact that the impulse magnitude increases as the angular velocity increases. The magnitude of the lateral displacement, however, becomes very large as the angular speed reaches 10 rad/s. So, the result might exceed the valid limit of the linear model. It can also be observed from the figure that the modal characteristics vary as the angular velocity varies. To clarify the fact, energy distribution versus frequency is calculated by using discrete Fourier transform. As shown in Fig. 3, the natural frequencies increase as the angular velocity increases. This is the well known phenomena which are often called as the stiffening effects. It can be also shown clearly in the figure that the energy distribution increases as the angular velocity increases.

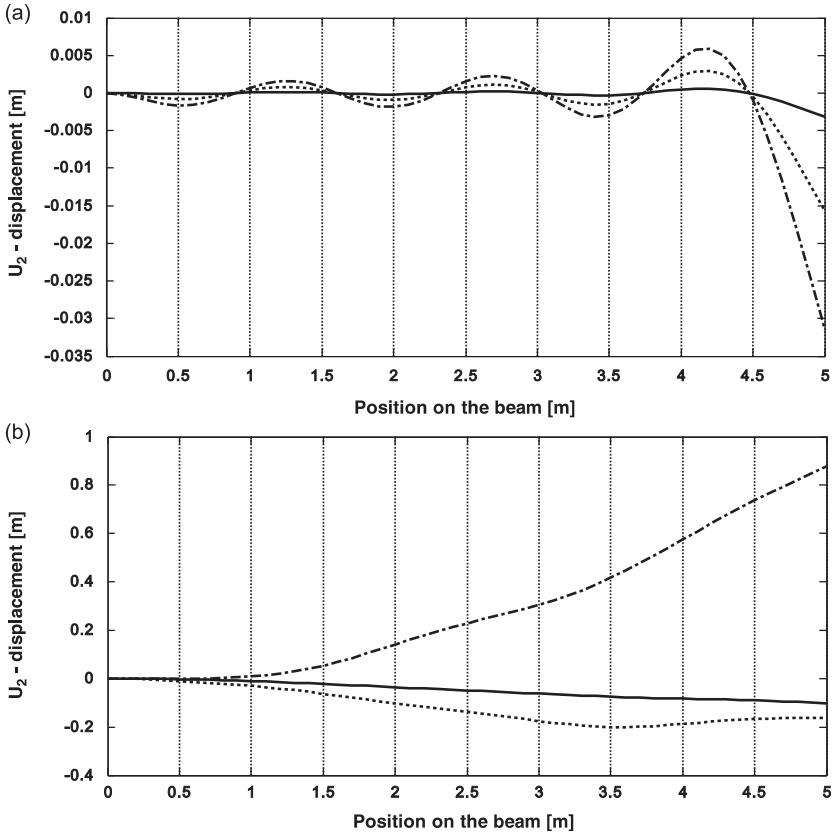

Fig. 4. Variation of beam shape induced by the impact with different angular velocity ($e = 1$, $a = 5\,\text{m}$, $t_I = 1\,\text{s}$, $m = 0.1\,\text{kg}$): (a) $t = 1.001\,\text{s}$. (b) $t = 3\,\text{s}$. —— $\omega_3 = 1\,\text{rad/s}$, ····· $\omega_3 = 5\,\text{rad/s}$, –·– $\omega_3 = 10\,\text{rad/s}$.

Fig. 4 shows the shapes of beam after the impact with different values of angular velocity. Fig. 4(a) shows the shape of the beam just after the impact. The highest frequency mode (7th bending mode) appears clearly in the figure. This simply indicates that 7 bending modes are employed to obtain these numerical results. Fig. 4(b) shows the shape of the beam at $t = 3\,\text{s}$. As shown in the figure, the lowest few modes dominate the dynamic response of the beam after some lapse of time while the effects of higher frequency modes decrease fast.

Fig. 5 shows the lateral tip deflection of the rotating beam undergoes constant angular velocity with three different impact locations. As the impact location approaches toward the fixed end of the cantilever beam, the peak deflection at the tip decreases. This simply results from the fact that the magnitude of impulse decreases as the impact location approaches toward the fixed end of the beam. Fig. 5 also shows that the impact location does not affect the natural frequencies of the rotating beam. Fig. 6 shows the variation of energy magnitude to be delivered at beam due to the impact versus impact locations. As the impact location moves toward the fixed end of the beam, energy magnitude to be delivered at beam due to the impact decreases. The energy ratio distribution versus frequency obtained by using discrete Fourier transform is shown in Fig. 7. As discussed previously, the natural frequencies do not vary with the impact location change. However, as the impact location moves toward the fixed end of the beam, the higher frequency energy portion increases while the lower frequency energy portion decreases.

Fig. 8 shows the shape of beam after the impact with different impact locations. Fig. 8(a) shows the shape of beam just after the impact. As shown in the figure, the deflection peaks are located at the locations of impact. Fig. 8(b) shows the shape of beam at $t = 3\,\text{s}$. As shown in the figure, the shapes for the impact locations $a = 3$ and 5 m are dominated by a few lowest modes. However, in the shape for the impact location $a = 1\,\text{m}$, the first mode is not well observed. This indicates that the higher frequency modes contribute more as the impact location approaches to the fixed end.

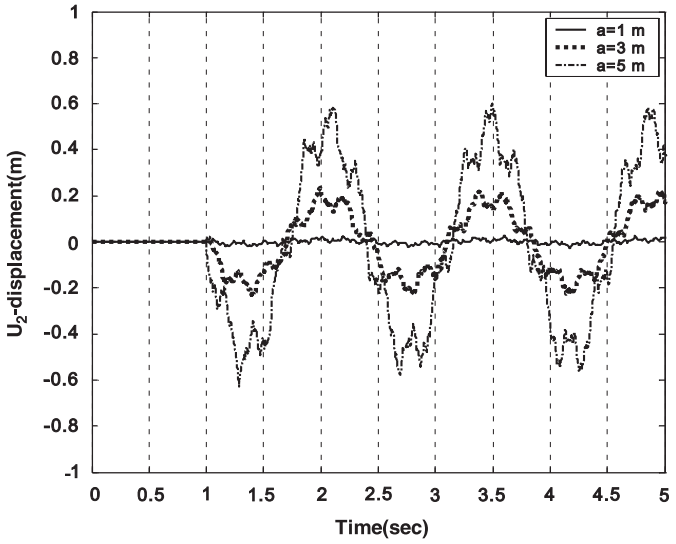

Fig. 5. Variation of beam tip deflection induced by the impact with three different impact locations ($e = 1$, $t_I = 1$ s, $\omega_S = 5$ rad/s, $m = 0.1$ kg): —— $a = 1$ m, ⋯⋯ $a = 3$ m, –·– $a = 5$ m.

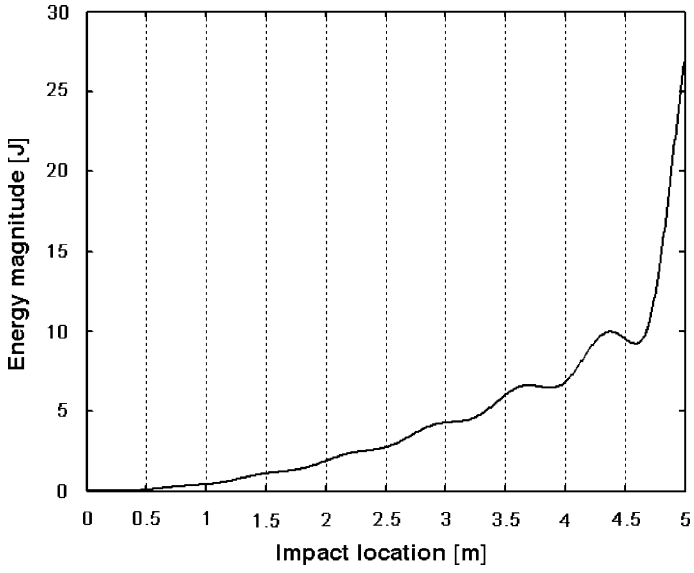

Fig. 6. Energy magnitude to be delivered at beam due to the impact versus impact locations ($e = 1$, $t_I = 1$ s, $\omega_S = 5$ rad/s, $m = 0.1$ kg).

Fig. 9 shows the variation of the particle mass velocity after collision versus particle mass size at rotating beam of the constant angular velocity. As shown in the figure, the velocity of the particle mass after collision decreases as the particle mass size increases. As the ratio of the particle mass to the beam mass approaches to zero, the velocity of the particle after impact approaches to a value. The value (when the particle mass size is very small compared to the beam mass) can be obtained from Eq. (14) as follows:

$$m \to 0 \Rightarrow \bar{v}_m = \omega_3(r + a)(e + 1),$$
$$m \to \infty \Rightarrow \bar{v}_m = 0. \tag{17}$$

For instance, if the coefficient of restitution between the beam and the particle is 1, the velocity of the particle after impact is twice the velocity of the impact point of the beam just before the impact occurs.

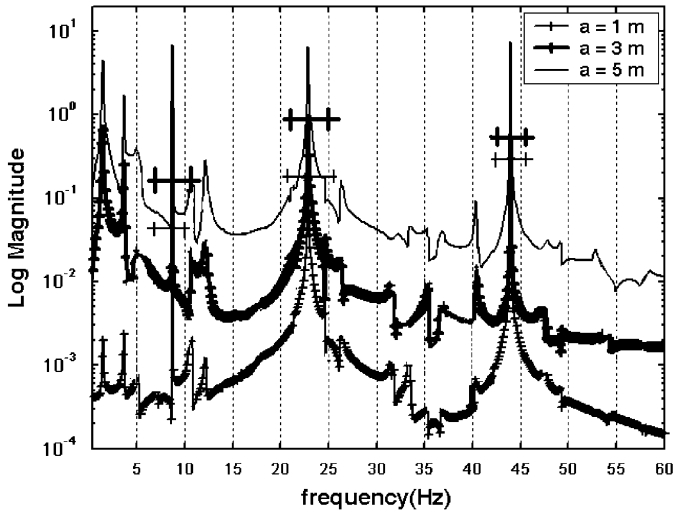

Fig. 7. Energy ratio distribution versus frequency after the impact and impact locations ($e = 1$, $t_I = 1\,\text{s}, \omega_S = 5\,\text{rad/s}$, $m = 0.1\,\text{kg}$): —┼— $a = 1\,\text{m}$, —╋— $a = 3\,\text{m}$, —— $a = 5\,\text{m}$.

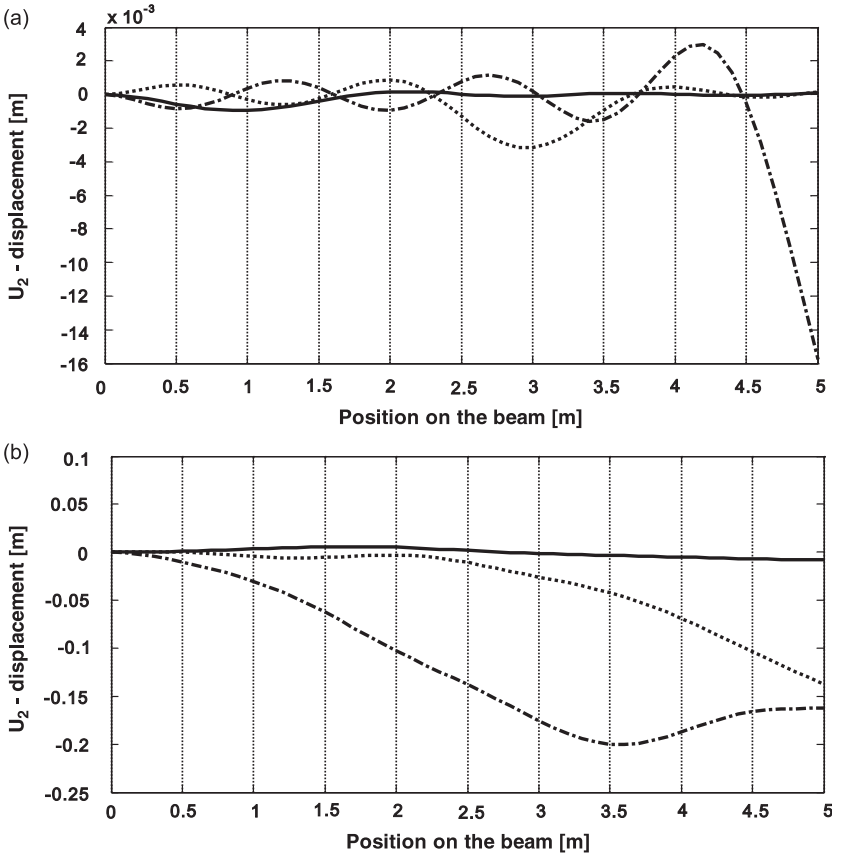

Fig. 8. Variation of beam shape induced by the impact with three different impact location ($e = 1$, $t_I = 1\,\text{s}$, $\omega_S = 5\,\text{rad/s}$, $m = 0.1\,\text{kg}$): (a) t = 1.001 s. (b) $t = 3\,\text{s}$. —— $a = 1\,\text{m}$, ⋯⋯ $a = 3\,\text{m}$, –·– $a = 5\,\text{m}$.

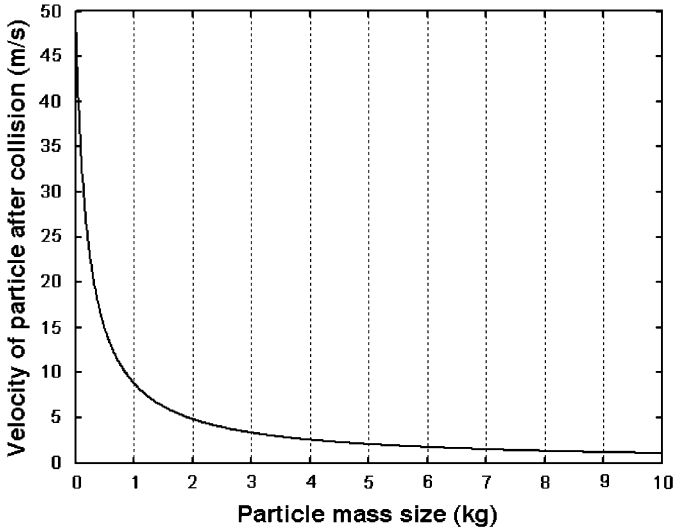

Fig. 9. Variation of the particle mass velocity after collision versus particle mass size ($e = 1$, $a = 5\,\text{m}$, $t_I = 1\,\text{s}$, $\omega_S = 5\,\text{rad/s}$).

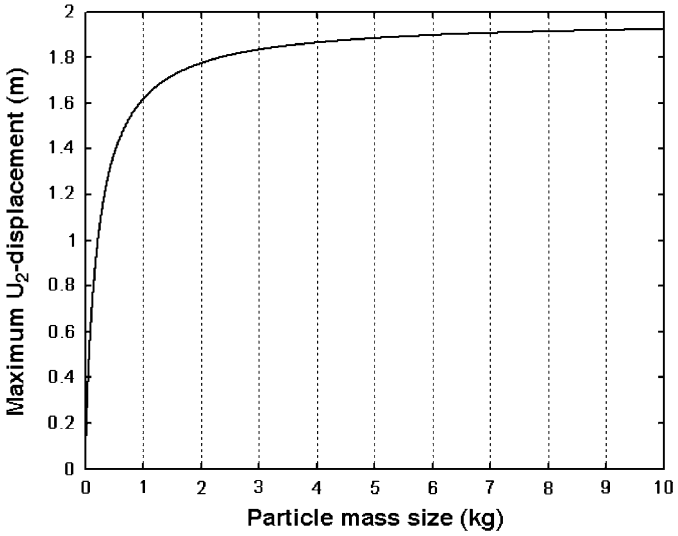

Fig. 10. Variation of maximum U-displacement in tip versus particle mass size with impact ($e = 1$, $a = 5\,\text{m}$, $t_I = 1\,\text{s}$, $\omega_S = 5\,\text{rad/s}$).

Fig. 10 shows the variation of the maximum tip deflection of the beam versus the particle mass size at rotating beam of the constant angular velocity. As shown in the figure, maximum tip deflection increases as the particle mass increases. However, the maximum value converges to a constant value as the particle mass increases. The impulse which is related to the maximum displacement can be also obtained as follows:

$$m \to 0 \Rightarrow I_{mp} = 0,$$
$$m \to \infty \Rightarrow I_{mp} = \frac{\rho_b L \omega_3 (r + a)(e + 1)}{\Sigma \phi_{2i}(a) \phi_{2i}(a)} \tag{18}$$

Fig. 11 shows the variation of maximum tip deflection and the particle mass velocity after collision versus coefficient of restitution at rotating beam of the constant angular velocity. As shown in the figure, the particle

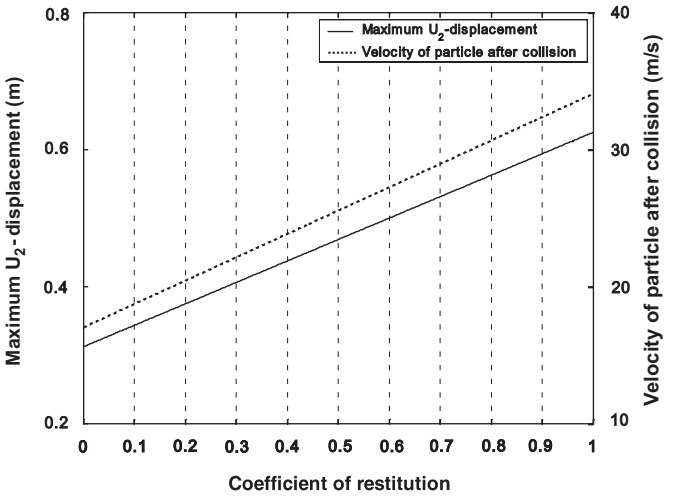

Fig. 11. Variation of maximum deflection and the particle mass velocity after collision versus coefficient of restitution ($a = 5\,\text{m}$, $\omega_S = 5\,\text{rad/s}$, $m = 0.1\,\text{kg}$): —— maximum U-displacement, ⋯⋯⋯ velocity of particle after collision.

mass velocity after collision increase linearly as the coefficient of restitution increases. This can be easily explained from Eq. (17). It can be also shown in the figure that maximum tip deflection increases as the coefficient of restitution increases. This fact can be also explained from Eq. (18). As the magnitude of impact increases, the deflection of the beam should be increased. Such beam deflection will often cause excessive stress and eventual failure of the structure. Thus, such information is very important for the design of a rotating structure, which is often collided by a particle mass.

4. Conclusion

In this paper, a modeling method for the dynamic analysis of a rotating beam collided by a particle mass is presented. The numerical results show that the beam deflection after impact increases as the angular speed of the beam increases. The well-known stiffening effect due to rotational motion is also observed from the results. As the location of collision approaches toward the fixed end of cantilever beam, the lateral deflection decreases. This results from the fact that the magnitude of impulse is influenced by the velocity of the impact point of the beam. It is also shown that lower frequency energy portion decreases while higher frequency portion increases as the location of collision approaches toward the fixed end of cantilever beam. As the rate of the particle mass to the beam mass approaches to zero, the velocity of the particle after impact is $1 + e$ times the velocity of the impact point of the beam just before impact. As the particle mass increases, maximum tip deflection approaches to a constant value.

Acknowledgments

This research was supported by Center of Innovative Design Optimization Technology (iDOT), Korea Science and Engineering Foundation.

References

[1] R. Southwell, F. Gough, The free transverse vibration of airscrew blades, *British A. R. C. Reports and Memoranda, No. 766*, 1921.
[2] M. Schilhansl, Bending frequency of a rotating cantilever beam, *Journal of Applied Mechanics—Transactions of the ASME* 25 (1958) 28–30.
[3] S. Putter, H. Manor, Natural frequencies of radial rotating beams, *Journal of Sound and Vibration* 56 (1978) 175–185.
[4] R. Bhat, Transverse vibration of a rotating uniform cantilever beam with tip mass as predicted by using beam characteristic orthogonal polynomials in the Rayleigh–Ritz method, *Journal of Sound and Vibration* 105 (1986) 199–210.

[5] H.H. Yoo, R.R. Ryan, R.A. Scott, Dynamics of flexible beams undergoing overall motions, *Journal of Sound and Vibration* 181 (1995) 261–278.
[6] J.M. Solberg, P. Papadopoulos, A finite element method for contact/impact, *Finite Elements in Analysis and Design* 30 (1998) 297–311.
[7] L. Demkowicz, A. Bajer, Conservative discretization of contact/impact problems for nearly rigid bodies, *Computer Methods in Applied Mechanics and Engineering* 190 (2001) 1903–1924.
[8] X. Zhang, L. Vu-Quoc, Modeling the dependence of the coefficient of restitution on the impact velocity in elasto-plastic collision, *International Journal of Impact Engineering* 27 (2002) 317–341.
[9] L. Vu-Quoc, L. Lesburg, X. Zhang, An accurate tangential force–displacement model for granular-flow simulations: contacting spheres with plastic deformation, force driven formulation, *Journal of Computational Physics* 196 (2004) 298–326.
[10] M. Anghileri, L. Castelletti, F. Invernizzi, M. Mascheroni, A survey of numerical models for hail impact analysis using explicit finite element codes, *International Journal of Impact Engineering* 31 (2005) 929–944.